Hydro–mechanical analysis of embankments stability in partially saturated soils under rainfall events

Gorizia D'Alessio[1,*], *Leonardo Maria* Lalicata[2], and *Francesca* Casini[1]

[1] University of Rome "Tor Vergata", Department Civil Engineering and Computer Science, via del Politecnico 1, 00133, Rome, Italy
[2] University of Genova, Department of Civil Environmental and Chemical Engineering, via Montallegro, 1, 16145 Genoa, Italy

Abstract. Road and railway embankments are often constructed in partially saturated conditions and their water content can change over time according to rainfall events and ongoing interactions with the atmosphere. These changes may trigger instability phenomena due to the reduction of suction as the wetting front advances. Conventional slope stability assessments often overlook these changes and assuming either dry or fully saturated conditions, which could lead to inaccurate predictions. In this work, coupled hydro-mechanical analyses were carried out on clayey and sandy soils to investigate the response of the soil during rainfall on the shape of the infiltration profile, which in turn, control the stability of the slope. The analyses were carried out with PLAXIS 2D adopting an elasto-plastic constitutive law, with Mohr - Coulomb strength criterion and Bishop's effective stresses. The water retention curve and the permeability law were described by using the Van Genuchten model. Slope stability was determined using the φ-c reduction method. The results showed that, as expected, the degree of saturation and the suction profiles have a significant influence on the stability of the slope and, therefore, neglecting them can lead to incorrect design and/or prediction of behaviour during the slope service life. Moreover, the observation of the shape of the suction profiles from the numerical analysis led to the validation of paradigmatic infiltration profiles, which can be used to perform uncoupled limit equilibrium analyses accounting for the partial saturation condition in a simplified and yet effective way. A novel design chart is introduced to describe the interplay between the slope's hydromechanical parameters, geometry, groundwater table position, and infiltration profile. Such stability chart correlates the safety factor to the slope inclination and to the mechanical parameters of the soil, as well as to the apparent cohesion induced by the partial saturation in the unsaturated portion of the slope.

1 Introduction

Road and railway embankments are typically compacted at gravimetric water contents below saturation, often close to the Proctor optimum [1]. In this state, the soil remains partially saturated, exhibiting higher strength compared to fully saturated or dry conditions. However, variations in water content during service life due to rainfall or fluctuations in the groundwater level can diminish this enhanced resistance, potentially leading to instability [2],[3]. Existing design charts for slope stability often rely on simplified models, frequently neglecting the effects of partial saturation above the ground water table. While recent studies have extended their scope to partially saturated soils, incorporating different suction profiles, these approaches still face limitations in generalisation. For instance, [4] and [5] restricted their analysis to slip surfaces that exit at the embankment toe, thereby excluding from the outset any possibility of intersection with the water table. Additionally, the solutions proposed by [5] and [6] consider only constant initial suction and degree of saturation profiles within the embankment.
To provide a comprehensive understanding of the problem, this paper presents the results of a systematic investigation into the relationship between embankment stability and partial saturation. Furthermore, the effect of infiltration from the ground surface is examined by applying simplified suction profiles on the limit equilibrium analysis. The results, validated through numerical analyses, yield to dimensionless stability charts based on the key geometrical, physical, mechanical and hydraulic properties of the embankment.

2 Methodology

The stability of the embankment under partially saturated conditions was investigated through an integrated approach, combining numerical analyses and limit equilibrium methods.

2.1. Numerical modelling

Fully coupled hydro-mechanical analyses were carried out using the finite element program PLAXIS 2D to assess the evolution of the suction profile within the embankment in function of the precipitation and the soil type. To that end, the analyses are conducted for both a

* Corresponding author: gorizia.d.alessio@uniroma2.it

sandy and a clayey soil assuming typical values of the hydro-mechanical parameters.

2.1.1 Model geometry, boundary and initial conditions

The homogeneous slope was 5m high with an inclination of 30°. The dimensions of the model (22.60m long × 10m high) were large enough to avoid boundary effects. The initial conditions were established by imposing a constant hydraulic head at the base of the domain, setting the ground water table, GWT, 3m below the toe of the slope. Consequently, the pore water pressure profile followed a hydrostatic distribution, while the lateral boundaries were modelled as permeable.

2.1.2 Constitutive model and hydraulic parameters

An elasto-plastic constitutive law with a Mohr-Coulomb criterion (Eq.1) for partially saturated soils was used, based on Bishop's effective stresses (Eq. 2) as follows:

$$\tau = \sigma'_n \tan \phi' + c' \quad (1)$$

$$\sigma'_n = (\sigma_n - u_a) + \chi (u_a - u_w) \quad (2)$$

Where σ_n and σ_n' are, respectively, the effective and the total stresses, normal to the plane on which the tangential stress τ is evaluated, c' is the effective cohesion, u_a is the air pressure and u_w is the pore water pressure and, finally, χ is the Bishop parameter which depends on degree of saturation. When the soil is fully saturated, the χ parameter is equal to 1 and the Bishop effective stresses recover those of Terzaghi. In this study, the Bishop parameter is taken to be equal to the effective saturation degree $S_e=(S_r-S_{res})/(S_{sat} - S_{res})$. The soil water retention curve (SWRC - Eq. 3) and the hydraulic conductivity function (HCF - Eq. 5) were described using Van Genuchten model [7], as given below:

$$Sr = S_{res} + S_e (1+(s/P)^n)^{-m} \quad (3)$$

$$K_{unsat} = k_{rel} K_{sat} \quad (4)$$

$$k_{rel} = S_e^{l} ((1-(1-S_e^{1/m})^m)^2 \quad (5)$$

Where S_{res} is the residual saturation degree, s is the suction, P is the air entry value, K_{unsat} is the hydraulic conductivity in unsaturated conditions, k_{rel} is the relative permeability, and K_{sat} is the saturated permeability. Finally, n and m (equal to $1-1/n$) are the model parameters. Table 1 summarises the mechanical and hydraulic parameters used in the numerical analyses for both sandy and clayey soils.

2.1.3 Calculation phases

Infiltration profiles were obtained through fully coupled numerical analyses, applying uniform rainfall conditions at the soil surface. Rainfall intensity was set equal to 0.86 mm/day for the clay soil, corresponding to a q/K_{sat} ratio of 10, and to 100 mm/day for the sand soil, representing an intense but realistic rainfall. The safety factor was then computed at the end of each rainy-day using $c' - \phi'$ reduction method, already implemented in the FEM code. In this method, the shear strength parameters (friction angle ϕ' and effective cohesion c') are progressively reduced until slope failure occurs. The safety factor is defined as the ratio of the available strength to the strength at failure and provides a measure of the overall stability of the slope [8], [9].

Table 1. Mechanical and hydraulic parameters used in the numerical analyses.

	SAND	CLAY
SOIL PARAMETERS		
Saturated unit weight γ_{sat} (kN/m^3)	18	18
Unsaturated unit weight γ_{unsat} (kN/m^3)	6	16
Friction angle ϕ' (°)	33	28
Effective cohesion c' (kPa)	0	5
Young modulus E' (MPa)	50	20
Poisson ratio ν (-)	0.30	0.30
SWRC - HCF		
Saturated permeability K_{sat} (m/s)	1e-5	1e-8
Air entry value P (kPa)	5	200
Van Genuchten parameter n (-)	1.80	1.56
Van Genuchten parameter l (-)	0.50	0.50
Residual saturation degree S_{res} (-)	0.10	0.20

2.2 Limit Equilibrium Method

The stability of the embankments under partial saturation conditions was assessed using Bishop's slice method [10], which assumes a circular slip surface. Bishop's approach is an established limit equilibrium method (LEM) recognised by Eurocode 7 [11] and, for homogeneous slopes, provides an optimal balance between computational speed and accuracy. The analysis was implemented in Python following the scheme shown in Fig. 1a, where H and β represent the embankment height and slope angle, respectively. For the sake of simplicity, the water table level H_w is assumed horizontal and it was measured vertically from the embankment toe, while the infiltration depth, z_w, is assumed parallel to the slope surface as suggested by [5]. The parameter z_w corresponds to the maximum depth at which pore pressure variations occur due to water infiltration. As widely accepted in the geotechnical community, the water pressure distribution and the saturation degree play a fundamental role in the stability of unsaturated slopes. Two cases of pore pressure distributions are considered in this study, as shown in Fig. 1b. The first is a constant pore pressure distribution representative of initial as-compacted or short-term embankment conditions, and the second is a hydrostatic pore pressure distribution corresponding to idealised long-term conditions. During rainfall, suction profile reduces near the ground surface due to water infiltration.

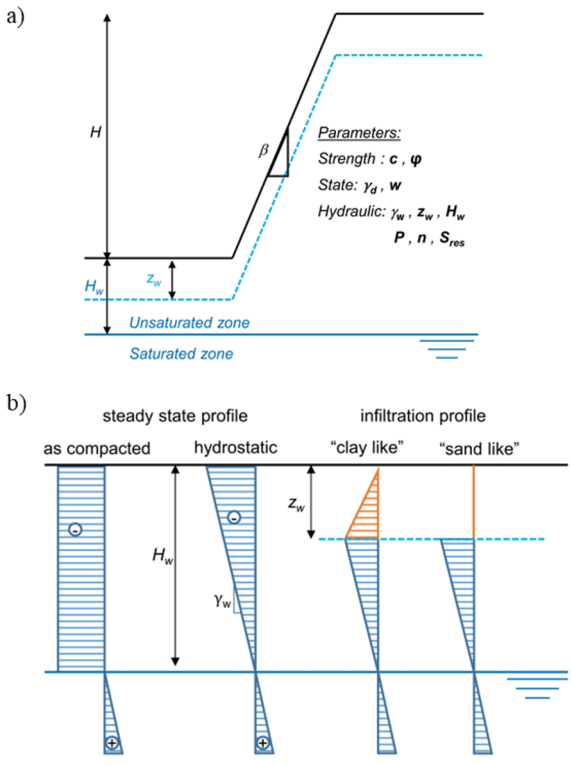

Fig. 1. a) Geometry assumed in the limit equilibrium model, b) Pore pressure profiles in the case of steady state conditions and in the case of infiltration.

Numerical modelling of fluid flow in porous media can be approached with varying levels of complexity. While transient finite element flow analyses provide precise results [12], their practical applicability is often limited by data requirements (e.g. permeability functions and precipitation data) and modelling assumptions (initial and/or boundary conditions). To address these limitations, this study adopts the wetting front infiltration model, which has demonstrated good agreement with both transient finite element analyses [13] and experimental observations [14][15]. The idealised infiltration profiles used in this work (Fig. 1b) are similar to those proposed by [5]. For clay-type soils, the suction profile is assumed to be zero at the ground surface and to increase linearly with depth, reaching the initial hydrostatic value at the infiltration depth. (z_w). In contrast, the sand-type profile maintains zero suction throughout the wetted zone. The position of z_w evolves in time as a function of rainfall intensity, soil permeability, and initial saturation state. Although standard one-dimensional infiltration models can predict this parameter [16], the current study treats z_w as an input variable, with its specific determination left to the reader. The validity of any selected infiltration depth must be carefully evaluated for each case, considering the specific boundary conditions and hydraulic properties of the soil. In this work, the WRC is described by the Van Genuchten model (Eq. 3) and, for the sake of simplicity, the hydraulic hysteresis is neglected. Table 2 shows typical values of WRC model parameters (P, n, S_{res}) for different soil types derived from the literature [17].

Table 2. Typical values of the WRC parameters for the Van Genuchten model.

SOIL	P (kPa)	n (-)	S_{res} (-)
Clay	25 – 1000	1.05 – 1.70	0.10 – 0.20
Silt	10 – 100	1.30 – 2.70	0.08 – 0.15
Sand	0.50 – 20	1.50 – 4.00	0.05 – 0.10

In the LE method, the soil strength is described by the Mohr - Coulomb failure criterion extended to the unsaturated state (Eq. 1), using Bishop's effective stresses (Eq. 2). Moreover, model explicitly account for the dependency of the soil unit weight γ on the dry unit weight γ_d and the water content w (Eq. 6):

$$\gamma = \gamma_d (1+w) \tag{6}$$

3 Results and discussion

3.1 Validation of infiltration profiles

Contours of pore pressure distribution and plastic deformations obtained from the FE analysis are presented in Fig. 2 at different times for the sand and clay soils, respectively. Inspection of Fig. 2 shows that, for both the soil types, the wetting front advances parallel to the soil surface. As an insight, Figure 3 compares the computed water pressure profiles at the centre of the embankment, at the same time steps as in Fig. 2, with the paradigmatic infiltration profiles adopted in the LE method. The position of the wetting front is easily recognised in the sand case, with a value of pore water pressure close to 0kPa (Fig. 3a). Conversely, for the clay case, there is a linear decrease in pore pressure in the wetting front, from 0 kPa to the soil surface, until the hydrostatic profile is reached (Fig. 3b). The results reported in Fig. 2 and Figure 3, confirm the validity of the infiltration profiles assumed for the LE method and shown in Fig. 1b. Fig. 4 shows the safety factor (F) evolution with the advancing infiltration depth (z_w). The limit equilibrium model, based on the simplified infiltration profiles, agrees well with the numerical results. For the sand case (Fig. 4 - squared markers), F gradually decreases from 1.97 at z_w=0 to 1.90 at z_w=0.7m, then drops more rapidly and stabilises around F~1.55 beyond z_w=1.2m. For the clay, (Fig. 4 - rounded markers), F decreases slowly until z_w~2.5m, then decreases more rapidly. These trends reflect the different pore pressure profiles computed upon infiltration (Fig. 3) and their interaction with the slip surface. When the wetting front reaches the slip surface, the decrease in F is more pronounced. The good agreement between the FEM and the LEM is demonstrated in Fig. 2 in terms of the shape of the slip surface. This consistency is further supported by the low mean errors in the F-values, which are equal to 4.7% for sand and 1.4% for clay.

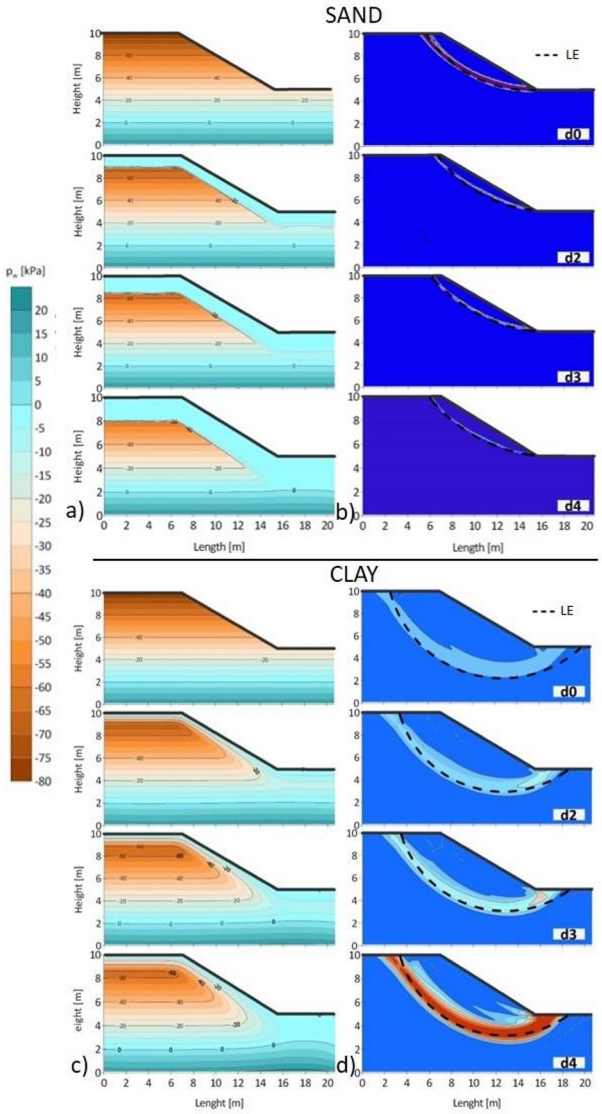

Fig. 2. Pore water pressure and plastic deformations contours for a,b) sand and c,d) clay.

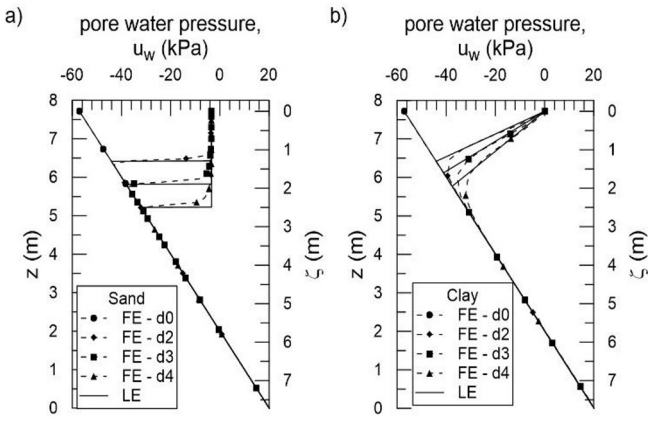

Fig. 3. Comparison between FEM and LEM results, in terms of pore pressure distribution: a) sand case, b) clay case.

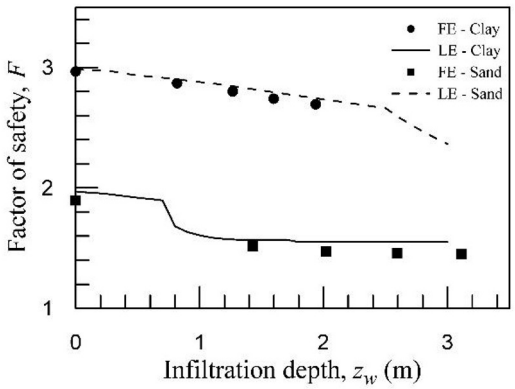

Fig. 4. Comparison between FEM and LEM results, in terms of F.

3.2 Stability charts

3.2.1 Steady state conditions

As-compacted embankments are characterised by a constant value of water content, and thus by a constant value of apparent cohesion (defined as $c_{app}=S_e s\tan\phi'$). Stability design charts can be presented in dimensionless form linking the normalised safety factor $F/\tan\phi'$ to a non-dimensional group, $c/\gamma H\tan\phi'$, which is function of the geometrical and the mechanical properties of the soil, and to the slope inclination β [6]. Fig. 5 shows the stability chart for unsaturated soils, together with typical ranges of the parameter $c/\gamma H\tan\phi'$ according to the different water retention parameters, evaluated for three soil types: sand, silt and clay. For the sake of simplicity, the effective cohesion c' is taken equal to 0kPa. Consequently, the cohesion c ($= c'+S_e s\tan\phi'$) only considers the apparent cohesion induced by the partial saturation. Optimum water content and dry density values are based on typical embankment construction data, and suction interval for each material is evaluated using retention curve parameters in Table 2. Finally, H ranges between 2 and 10 m, and the resulting values are summarised in Table 3. From the inspection of Table 3, it is clear that for clays the upper limit of the dimensionless apparent cohesion $S_e s/\gamma H$ is very high, mainly due to the high P values (up to 1000 kPa) that a clay can reach. However, these values are typically observed for fine and active clays, which are not suitable for embankment construction. For the sake of safety and simplicity, an average value of 4 can therefore be considered. The stability chart in Fig. 5 provides the value of F, given the characteristics of the embankment such as geometry and soil type. Due to the reduced retention capacity, the increase in strength of a partially saturated sandy soil is significantly lower than that of a silty or clayey soil, as shown by the upper limits of the dimensionless apparent cohesion in Fig. 5. On the other hand, in a silty soil, the influence of partial saturation, expressed by the parameter $S_e s/\gamma H$, can vary from 0 to 1.3. This means that for a 5m high embankment with a 30° inclination, partial saturation can increase stability by up to 590% compared to dry conditions.

Table 3: Typical values for as-compacted embankments

SOIL	SAND	SILT	CLAY
Optimum water content w (-)	0.60	0.12	0.16
Optimum dry density γ_d (kN/m^3)	21.80	19.00	17.50
Unit weight γ (kN/m^3)	23.10	21.30	20.30
Degree of saturation S_r (-)	0.81	0.85	0.86
Range of $S_e s/\gamma H$ (-)	[0.01 - 0.40]	[0.03 – 1.30]	[0.30 – 100]
Mean value of $S_e s/\gamma H$ (-)	0.20	0.75	4.00

The stability chart can be used as long as the distribution of the degree of saturation can be considered constant within the embankment, i.e. immediately after construction, or when the soil is close to the residual conditions of the retention curve. In all other cases, such as under hydrostatic conditions, and under infiltration or evaporation, the chart may no longer be valid a priori, and therefore a stability analysis, considering an appropriate pore water pressure distribution, can be necessary. An example of the effects of the infiltration profile is given in the following section.

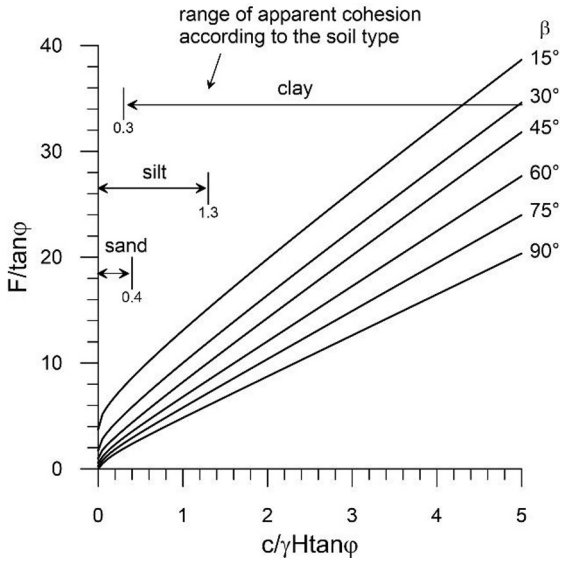

Fig. 5. Stability chart for partially saturated embankments

3.2.2 Infiltration profiles

An example of the influence of the infiltration profile on the stability of an embankment is shown in Figure 6, for an embankment with H=5m, β=60° and non-dimensional apparent cohesion $S_e s/\gamma H$=0.38. Two analyses were carried out considering both the "sand-like" and the "clay-like" infiltration profile. The hydromechanical parameters of the silty soil (Table 2) are the same in both analyses. In absence of infiltration (z_w=0) F is equal to 1.78 (F/tanϕ'=3.35), and for the "sand-like" infiltration profile, instability occurs when z_w/H=0.18 (corresponding to F/tanϕ=0.58). Differently, for the "clay-like" infiltration profile, the safety factor F decreases slowly as the wetting front advances. This is because the suction within the wetting front, and therefore the apparent cohesion, remains always larger than zero. At z_w/H~0.42, a change in the evolution of F is observed, because after this point the entire slip surface is included in the wet zone, causing a significant reduction in the apparent cohesion available for stability analysis. The depth z_w at which the evolution of F changes, is called "transition infiltration depth" (or simply "transition depth"). This depth marks the transition between a slip surface not significantly affected by the wetting front and a slip surface entirely comprised within the wetting front. In the case analysed, the transition depth depends on the infiltration profile and it is equal to 0.2H and 0.42H for the "sand-like" and the "clay-like" infiltration profiles, respectively. If the infiltration depth is smaller than the transition one, the factor of safety (F) can be determined using the stability chart with an averaged apparent cohesion across the height H, showing less than 6% variation compared to the LEM (Fig. 6a). Conversely, as z_w/H increases, the analysis deviates from the stability chart. In this case, it is necessary to carry out an appropriate slope analysis, taking into account the actual distribution of suction and the degree of saturation.

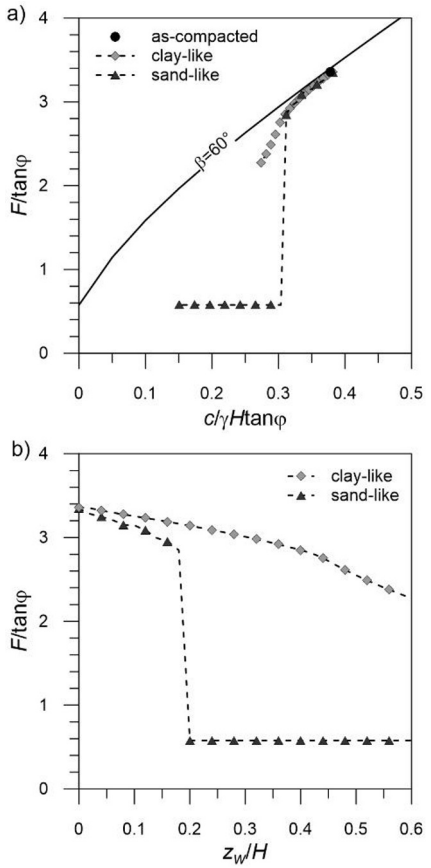

Fig. 6. Influence of infiltration profile on the stability of the embankment.

4 Conclusions

The stability of partially saturated embankments was investigated using a limit equilibrium method and assuming a simplified suction profile upon infiltration. Rainfall was modelled using different suction profiles based on soil type, validated by fully coupled hydromechanical numerical analyses. The proposed stability chart allows a direct assessment of the safety factor of an embankment with known geometry and hydromechanical properties, provided that the water content profile can be assumed to be constant. This chart remains accurate with minimal error even when the wetting front is relatively shallow (up to about 20% of the embankment height for "sand-like" infiltration profiles and 40% for "clay-like" profiles). However, when the wetting front penetrates deeper into the soil, a more detailed stability analysis is required, taking into account the actual pore pressure distribution. Although simplified, the wetting front concept provides a quick estimate of the stability of the embankment during rainfall events. This makes it a useful tool in the preliminary design stages.

The first author acknowledges MUR for supporting her fellowship through the PNRR-M4C1/DM 351 (09/04/2022).

References

[1]. N. Fatema, & M. Ansary. *Journal of Civil Engineering (IEB)*, 42(1), 119-136M. Ben Rabha, M.F. Boujmil, M. Saadoun, B. Bessaïs, Eur. Phys. J. Appl. Phys. (2014).

[2]. L. Cascini, M. R. Scoppettuolo, E. Babilio. *Landslides*, *19* (12), 2839–2851 (2022).

[3]. M. Pirone, R. Di Maio, G. Forte, C. De Paola, E. Di Marino, R. Salone, A. Santo, G. Urciuoli, G. *Engineering Geology*, *315*, 107045 (2023).

[4]. F. Vahedifard, D. Leshchinsky, K. Mortezaei, N. Lu. *International Journal of Geomechanics*, 16(6), D4016003 (2016).

[5]. W. Huang, E-C Leong, H. Rahardjo. *Journal of Geotechnical and Geoenvironmental Engineering*, 144(9), 04018066 (2018).

[6]. W. Huang. *International Journal of Geomechanics*, 23(9), 04023136 (2023).

[7]. van Genuchten, M.T. *Soil Science Society of America Journa*l, 44(5), 892–898. (1980).

[8]. T. Matsui, K.C. San. *Soils and foundations*, 32(1), 59-70. (1992).

[9]. E. M. Dawson, W. H. Roth, A. Drescher *Geotechnique*, 49(6), 835-840. https://doi.org/10.1680/geot.1999.49.6.835 (1999).

[10]. A. W. Bishop. *Géotechnique*, 5(1), 7–17 (1955).

[11]. A. J. Bond, B. Schuppener, G. Scarpelli, T.L.L. Orr. J*oint Research Centre, Institute for the Protection and Security of the Citizen.* Dimova, S. Pinto, A., Nikolova, B. Eds (2013).

[12]. S. Cuomo, A. Di Perna, M. Martinelli. *Engineering Geology*, 294, 106371 (2021).

[13]. L.M. Lee, N. Gofar, H. Rahardjo. *Engineering Geology*, 108(3–4), 272–285 (2009).

[14]. A. G. Li, Z. Q. Yue, L.G. Tham, C. F. Lee, T.K Law. *Canadian Geotechnical Journal*, 42(1), 13–26 (2005).

[15]. L. M. Lalicata, G. D'Alessio, F. Casini, *Transportation Geotechnics* https://doi.org/10.1016/j.trgeo.2025.101582 (2025).

[16]. J. W. Godt, B. Şener-Kaya, N. Lu, R. L. Baum. *Water Resources Research*, 48(5) (2012).

[17]. W. J. Likos, N. Lu, J.W. Godt. *Journal of Geotechnical and Geoenvironmental Engineering*, 140(4), 04013050. (2014).